

Fixed-point Inversion for Text-to-image diffusion models

Barak Meiri^{1,2*}, Dvir Samuel^{1,3*}, Nir Darshan¹, Gal Chechik^{3,4}, Shai Avidan², Rami Ben-Ari¹

¹OriginAI, Tel-Aviv, Israel

²Tel-Aviv University, Tel-Aviv, Israel

³Bar-Ilan University, Ramat-Gan, Israel

⁴NVIDIA Research, Tel-Aviv, Israel

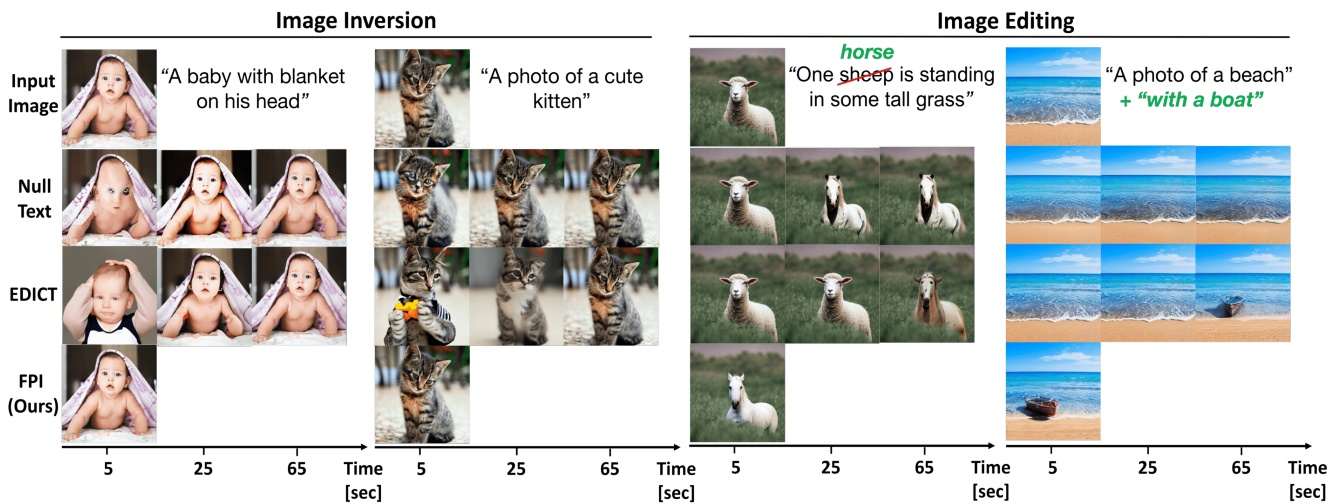


Figure 1. **Fixed-point Inversion (FPI) for real image inversion and editing:** FPI exhibits significantly faster performance compared to prior techniques with similar or better editing quality. By the time FPI completes the task, other methods are still in their intermediate stages.

Abstract

Text-guided diffusion models offer powerful new ways to generate and manipulate images. Several applications of these models, including image editing interpolation, and semantic augmentation, require diffusion inversion. This is the process of finding a noise seed that can be used to generate a given image. Current techniques for inverting a given image can be slow or inaccurate. The technical challenge for inverting the diffusion process arises from an implicit equation over the latent that cannot be solved in closed form. Previous approaches proposed to solve this issue by approximation or various learning schemes. Here, we formulate the problem as a fixed-point equation problem and solve it using fixed-point iterations, a well-studied approach in numerical analysis. We further identify a source of inconsistency that significantly hurts the inversion of real

images encoded to the latent space. We show how to correct it by applying a prompt-aware adjustment of the encoding. Our solution, **Fixed-point inversion**, is much faster than previous techniques like EDICT [22] and Null-text [13], with similar inversion quality. It can be combined with any pretrained diffusion model and requires no model training, prompt tuning, or additional parameters. In a series of experiments, we find that Fixed-point inversion shows improved results in several downstream tasks: image editing, image interpolation, and generation of rare objects.

1. Introduction

Text-to-image diffusion models [1, 15–17] can generate diverse and high-fidelity images based on user-provided text prompts. These models are further used in several important tasks that require *inversion*, namely, discovering an initial noise (seed) that, when subjected to a forward (denoising) diffusion process along with the prompt, generates the

*Equal Contribution.

Correspondence to: Barak Meiri <barak1908@gmail.com> or Dvir Samuel <dvirsamuel@gmail.com>.

input image. Inversion is used in various tasks including image editing [6], personalization [4, 5], seed noise interpolation [18] and generating rare concepts [19].

As inversion became a critical infrastructure block of various tasks, several inversion methods were developed. Primarily, Denoising Diffusion Implicit Models (DDIM) [21] introduced a deterministic sampling technique to map an initial noise seed into a generated image. Conversely, DDIM inversion uses that technique to transform an image into a latent noise representation by approximating the inversion equation. This approximation makes it very fast (~ 1.5 sec on a single A100 GPU), but it also introduces inconsistencies, (as explained in section 3.2), which causes a noticeable effect in generated images.

Several attempts have already been made to address these inconsistencies in DDIM Inversion. Null-text [13] aims to bring closer the diffusion states of the inversion process and the generation process, by adjusting the unconditional textual embedding used in classifier-free guidance [7]. EDICT [22] uses two coupled noise vectors to invert each other in an alternating fashion, to reach an exact diffusion inversion. Both Null-text and EDICT succeed in providing high-quality reconstruction results, but require a much higher computational cost: storing $3M$ or $16K$ parameters respectively for every inverted image, and running for 20 or 60 seconds per inversion, orders of magnitude slower than DDIM inversion.

In this paper, we address the problem of inversion inconsistencies with a fast, simple, yet fidelity-preserving procedure. Building on techniques from the field of numerical solution of equations, we take a simple fixed-point-iteration approach [2]. We name our approach FPI, for *Fixed-Point Inversion*. FPI enforces the consistent inversion of an image by applying only a few fixed-point iterations at each diffusion step. In particular, we demonstrate how fixed-point iteration theory can be used to solve the implicit functions introduced by DDIM. We show, that in practice, 2 to 5 iterations were already sufficient for convergence, yielding significantly more accurate results than DDIM inversion. FPI requires no model training or finetuning, no prompt optimization, or any additional parameters. It can be combined with all pre-trained diffusion models.

We also identify a second source of inconsistency, which significantly hurts inversion of real images. We find that when *real* images are encoded into the latent space, their encoding may misfit the inversion process since that process was designed to invert *generated* images for a given prompt. We show that applying a short prompt-aware adjustment of the encoding greatly improves inversion quality of FPI.

Figure 1 illustrates the quality and speed of FPI, for both reconstruction and editing. It inverts real images within 5 seconds, reaching similar or better quality than competing methods while being an order of magnitude faster.

We evaluate FPI extensively. First, we directly assess the quality of inversions found with FPI by measuring reconstruction performance, showing comparable results to [13, 22] but with $\times 4$ to $\times 12$ speedup gain. We then demonstrate the benefit of FPI in two downstream tasks (1) In *Image editing*, FPI smoothly changes fine details in the image in a consistent and coherent way, whereas previous methods struggle to do so. (2) In *Rare concept generation* with [19], and seed interpolation [18], that require diffusion inversion. In both of these tasks, FPI yields more accurate seeds, resulting in superior generated images using [18, 19].

2. Related work

Diffusion Model Inversion: Text-to-image diffusion models [1, 15–17] translate random samples (seeds) from a high-dimensional space, guided by a user-supplied text prompt, into corresponding images. DDIM [21], is a widely used deterministic scheduler, that demonstrates the inversion of an image to its latent noise seed. While effective, it was designed for unconditional diffusion models and lacked the capability to handle text prompts or editing. When applied to inversion for text-guided diffusion models, DDIM inversion suffers from *inconsistency*, particularly when the classifier-free guidance constant is large [13]. This happens due to its reliance on a linear approximation, causing the propagation of errors that result in inaccurate image reconstruction and the loss of content.

Recent studies [13] and [22] Address this limitation that arises from DDIM Inversion. Null-text inversion [13] improves reconstruction accuracy by optimizing the embedding vector of an empty string. This ensures that the diffusion process calculated using DDIM inversion, aligns with the reverse diffusion process.

[12] further incorporates the Null-Text Inversion approach by replacing the null-text embedding with a prompt embedding instead. This enhances convergence time and reconstruction quality but results in inferior image editing quality. In both [13] and [12], the optimized embedding must be stored, resulting in nearly 3 million additional parameters for each image when inverting with StableDiffusion v1.5 for 50 denoising steps.

EDICT [22] introduced invertible neural network layers, specifically Affine Coupling Layers, to compute both backward and forward diffusion paths. However, it comes at the cost of doubling the number of neural function evaluations (NFEs) compared to DDIM inversion, leading to prolonged runtime. Furthermore, additional latent has to be stored for every inverted image ($16K$ additional parameter per image in StableDiffusion [16]).

[23] proposed a novel scheme tailored for EDICT, referred to as bi-directional integration (BDIA). This approach aims to decrease the number of neural function evaluation (NFE) operations in EDICT while preserving accu-

rate diffusion inversion. While it provides examples with strong editing capabilities, it still demands an excessive amount of time ($\times 10$ than DDIM Inversion).

An alternative method proposed by [8] recommends modifying the noise maps to establish a stronger connection with the provided image, resulting in a non-Gaussian noise distribution. Nevertheless, this approach remains computationally expensive, requiring $\times 10$ time than DDIM Inversion. Furthermore, its applicability is restricted solely to editing tasks.

Seed Exploration & Rare concept generation: Here, we introduce another task that heavily relies on diffusion inversion. Generally, the data used for training diffusion models frequently has an unbalanced distribution of concepts [19]. This makes it hard for diffusion models to generate accurate images of rare concepts, and they often generate distorted images or images of closely related but different concepts (e.g. instead of "tiger cat", it generates a "tiger", see [19]). To overcome this limitation, SeedSelect [19] employs a small set of real images along with their corresponding seeds for seed optimization. This process iteratively refines a seed until a plausible image is generated by the diffusion model. A follow-up approach, NAO [18], introduced new interpolation paths (NAO-path) and centroids (NAO-centroid) of seeds as initialization for SeedSelect. NAO and SeedSelect both use DDIM Inversions for initial seed evaluation, which highly impacts results.

The current paper offers an alternative for obtaining precise inversion seeds for NAO and SeedSelect, in order to produce better images in terms of appearance and semantic accuracy. It's important to highlight that existing inversion techniques (Null-Text [13] and EDICT [22]) are not applicable in this context as they necessitate extra parameters for image reconstruction, which impedes the straightforward implementation of interpolation and centroid identification as suggested by NAO.

3. Method

3.1. Preliminaries

We first establish the fundamentals of Diffusion Denoising Probabilistic Models (DDPMs) and Denoising Diffusion Implicit Models (DDIMs). In these models, a *forward pass* (denoising) is the process that generates an image from a seed noise. A *backward pass* (inversion) is the process that, given an image, finds its corresponding seed noise.

Diffusion Denoising Probabilistic Models (DDPMs): DDPMs learn to generate images through a systematic process of iteratively adding Gaussian noise to a data sample until the data distribution is mostly noise. The data distribution is subsequently gradually restored through a reverse

diffusion process initiated with a random sample (noise seed) from a Gaussian distribution. In recent, *latent* diffusion models [1, 15–17], noising and denoising are applied to a latent representation of images derived from a variational autoencoder, rather than the images directly. Specifically, the process of mapping a (latent) image to noise is a Markov chain that starts with z_0 , and gradually adds noise to obtain latent variables z_1, z_2, \dots, z_T , following

$$q(z_1, z_2, \dots, z_T | z_0) = \prod_{t=1}^T q(z_t | z_{t-1}). \quad (1)$$

Each step in this process is a Gaussian transition

$$q(z_t | z_{t-1}) := \mathcal{N}(z_t, \sqrt{1 - \beta_t} z_{t-1}, \beta_t I), \quad (2)$$

parameterized by a schedule $\beta_0, \beta_1, \dots, \beta_T \in (0, 1)$. z_t can be expressed as a linear combination of z_0 and Gaussian noise $\varepsilon \sim \mathcal{N}(0, I)$:

$$z_t = \sqrt{\alpha_t} z_0 + \sqrt{1 - \alpha_t} \varepsilon, \quad (3)$$

where $\alpha_t = \prod_{i=1}^t (1 - \beta_i)$.

Text-guided diffusion models control the diffusion process with a control signal in the form of a latent representation p of a text prompt (often a CLIP embedding). A denoising network ϵ_θ aims to minimize the loss:

$$\mathcal{L} = \mathbb{E}_{z_0, \varepsilon \sim \mathcal{N}(0, 1), t} [\|\varepsilon - \epsilon_\theta(z_t, t, p)\|_2^2]. \quad (4)$$

The role of the denoising network ϵ_θ is to accurately eliminate the added noise ε from the latent code z at every time step t , based on the input of the noisy latent code z_t and the encoding of a conditioning text p .

Denoising Diffusion Implicit Models (DDIM). Sampling from diffusion models can be viewed alternatively as solving the corresponding diffusion Ordinary Differential Equations (ODEs) [10]. DDIM [21] scheduler, a popular deterministic scheduler, proposed denoising a latent noise vector in the following way:

$$z_{t-1} = \sqrt{\frac{\alpha_{t-1}}{\alpha_t}} z_t - \sqrt{\alpha_{t-1}} \cdot \Delta\psi(\alpha_t) \cdot \epsilon_\theta(z_t, t, p), \quad (5)$$

where $\psi(\alpha) = \sqrt{\frac{1}{\alpha} - 1}$, and $\Delta\psi(\alpha_t) = \psi(\alpha_t) - \psi(\alpha_{t-1})$.

The noise term ε that was added in Eq. (3) is replaced here with the output of the network $\epsilon_\theta(z_t, t, p)$ that was trained to predict it.

DDIM inversion: We now focus on inversion in the latent representation. Given an image representation z_0 and its corresponding text prompt p , we seek a noise seed z_T that, when denoised, reconstructs the latent z_0 . Several

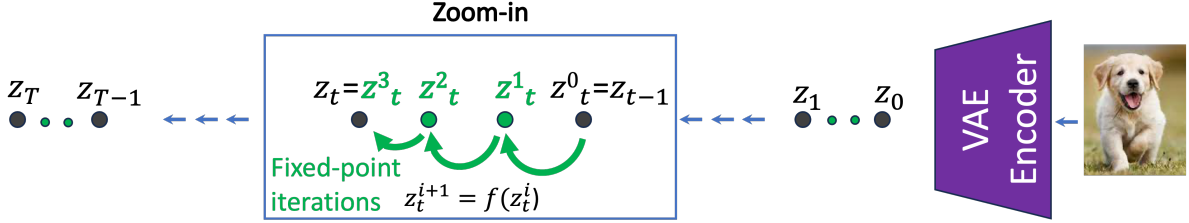


Figure 2. **Fixed-Point Inversion** iterates over an implicit function (Eq. 8), at every time step in the backward path. It starts with $z_t^0 = z_{t-1}$ and quickly converges to z_t . Each box denotes one inversion step; black circles correspond to intermediate latents in the denoising process; green circles correspond to intermediate fixed point iterations.

approaches were proposed for this task, and we focus on DDIM inversion. In this technique, Eq. (5) is rewritten as:

$$z_t = \sqrt{\frac{\alpha_t}{\alpha_{t-1}}} z_{t-1} + \sqrt{\alpha_{t-1}} \cdot \Delta\psi(\alpha_t) \cdot \epsilon_\theta(z_t, t, p). \quad (6)$$

This is an implicit equation in z_t that can be approximated by replacing z_t with z_{t-1}

$$\approx \sqrt{\frac{\alpha_t}{\alpha_{t-1}}} z_{t-1} + \sqrt{\alpha_{t-1}} \cdot \Delta\psi(\alpha_t) \cdot \epsilon_\theta(z_{t-1}, t, p). \quad (7)$$

The quality of the approximation depends on the difference $z_t - z_{t-1}$ (a smaller difference would yield a small error) and on the sensitivity of ϵ_θ to that z_t . See [3, 21] for details.

By applying Eq. (7) repeatedly for every denoising step t , one can invert an image latent z_0 to a latent z_T in the seed space. DDIM inversion is fast, but the approximation of Eq.(7) inherently introduces errors at each time step. As these errors accumulate, they cause the whole diffusion process to become inconsistent in the forward and the backward processes, leading to poor image reconstruction and editing [13, 22].

3.2. Fixed-point Inversion

We propose to replace the approximation of the inversion process of Eq. (7), by solving the implicit equation Eq. (6) directly. For that purpose, we propose using *fixed point iterations*, a common technique in the optimization of implicit equations [2]. Specifically, using upper-script i to denote iterations, we have:

$$\begin{aligned} z_t^0 &= z_{t-1} \\ z_t^{i+1} &= f(z_t^i), \end{aligned} \quad (8)$$

where

$$f(z_t) = \sqrt{\frac{\alpha_t}{\alpha_{t-1}}} z_{t-1} + \sqrt{\alpha_{t-1}} \cdot \Delta\psi(\alpha_t) \cdot \epsilon_\theta(z_t, t, p). \quad (9)$$

That is, given a z_{t-1} we perform fixed-point iterations to minimize the residual error of the implicit equation.

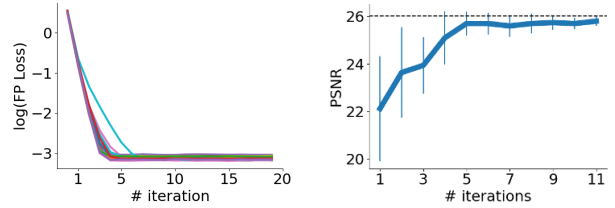


Figure 3. **Fixed-Point Iterations:** We measure the effect of the number of fixed-point iterations. **(Left)** The log loss of the error $f(x) - x$ for 50 images (plot for each image). It shows that FP-inversion converges for all images we tested. **(Right)** PSNR of reconstructed images, vs the maximum number of FP iterations. The dashed line represents the upper bound induced by Stable Diffusion VAE. It shows that FPI converges in only 2-3 iterations, reaching a PSNR closely approaching the upper limit established by the diffusion model VAE.

Figure 2 illustrates this process. The output of our method is a single latent z , similar to the DDIM Inversion’s output. Note that DDIM becomes a unique case of our scheme where the initial estimation z_t^0 is considered as the final output. As we show below, it leads to an improved reconstruction of the image in terms of PSNR with minimal run time overhead.

An advantage of our method is that we only modify the inversion process without altering the forward process of the diffusion model. This makes our method very easy to integrate into all diffusion models. Furthermore, this ensures that the reconstruction (forward) process remains as fast as the DDIM basic process, as it has not been altered.

More sophisticated methods are known for solving implicit functions like Newton-Raphson and Conjugate Gradient [14]. We found these methods to be impractical in this case due to the high dimensionality of the seed space or because they needed much more time to converge. Consequently, we opted for a simpler approach, which already achieves accurate solutions within a few iterations. Further details can be found in the supplementary material.

Convergence. Fixed-point iterations are guaranteed to converge if the operator is contractive in the region of interest. Formally, a mapping f is contractive on its domain if there exists $\rho < 1$ such that $\|f(x) - f(y)\| \leq \rho\|x - y\|$, $\forall x, y$, where $\|\cdot\|$ denotes any matrix norm. As a simple result, obtained by applying fixed-point iterations twice, the sequence of differences forms a monotonically reducing sequence: $\|x_2 - x_1\| = \|f(f(x_0)) - f(x_0)\| < \|f(x_0) - x_0\| = \|x_1 - x_0\|$.

In our case, it is not theoretically guaranteed that the function f is contractive everywhere. Luckily, the mapping may still be contractive in our region of interest. Indeed, we find that in practice, iterating Eq. (6) reduces the difference $\Delta z = z_t^i - f(z_t^i)$ (the equation residual) along the iterations. Figure 3(left) shows FPI loss (residuals) curves as a function of the number of iterations on a single diffusion step. Figure 3(right) depicts the effect of the number of running iterations on image reconstruction, in terms of PSNR. The figures illustrate that FPI converges in only 2-3 iterations, achieving a PSNR close to the upper bound set by the diffusion model VAE.

3.3. Fixed-point iterations for consistent inversion

We now focus on an important subtlety that greatly impacts inversion quality. Our inversion process is designed to agree with a generation process for a prompt p . However, inversion is typically applied to photos and images that are not generated by the model. Such an image x is mapped into the latent z_0 in a way that is unaware of the prompt because the VAE encoder is prompt-agnostic. This means that the typical input to our inversion process may be inconsistent with the prompt we use.

This problem is illustrated in Figure 4(a). Here, we randomly sampled z_T and ran the forward process with the prompt “A cute dog”. This results in a denoised latent z_0 which is decoded into an image x . Then, z_0^E is obtained by passing x through the encoder E . In terms of L_2 distance, z_0^E differs only slightly from z_0 , but it is not consistent with the prompt p (outside the dashed circle). As a result, applying inversion and reconstruction (dashed brown lines) from z_0^E yields a reconstructed latent \hat{z}_0^E that is far from z_0 . As a consequence, when z_0^E is decoded by the VAE, it results in a different image x' of “a cute dog”. This illustrates that inversion becomes inconsistent when applied to prompt-agnostic latents. To quantify this effect, we repeated this experiment for 10k images and found the mean L_2 distance between z_0 and \hat{z}_0^E ($\|z_0 - \hat{z}_0^E\|$) to be 99. In comparison, the mean distance between z_0 and z_0^E ($\|z_0 - z_0^E\|$) is only 16. This indicates that the inversion process produces latents that deviate significantly from the original z_0 .

How can this inconsistency be resolved? We propose to employ a short preprocessing step of another fixed-point iteration. The objective is to find a fixed point z_0 for the

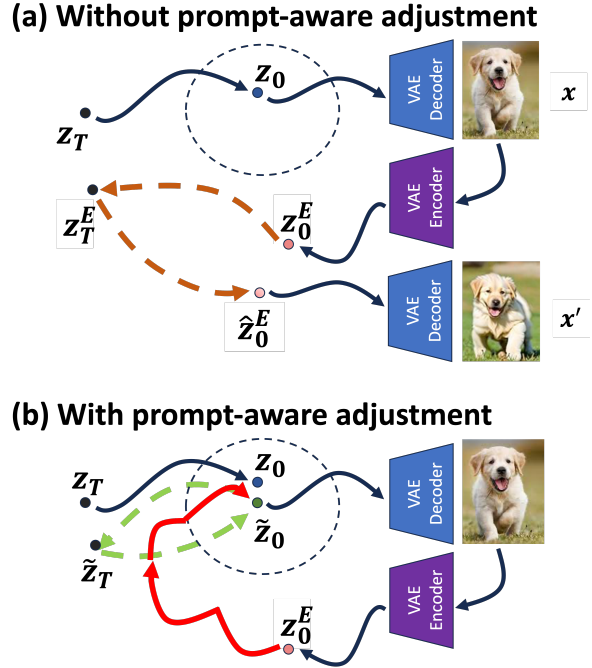


Figure 4. **Prompt-aware adjustment for more consistent inversion.** (a) A seed z_T is used to generate latent image z_0 , which is then decoded into an image x . If that image is encoded into the latent space $z_0^E = E(x)$, its representation z_0^E may not be aligned with the prompt used for inversion and generation (brown dashed line). As a result, the reconstructed \hat{z}_0^E differs significantly from z_0^E , yielding an inconsistent image x' . (b): Inconsistency can be fixed using a short noising and denoising step (red curves), which yields \tilde{z}_0 . Then, applying the complete backward-forward process (green curves) can generate a consistent \tilde{z}_0 .

implicit function $z_0 = h(z_0, p)$, with h representing the backward-forward process and p is the prompt that would be used for inversion. The initial guess for the fixed-point iterations is $z_0^E = E(x)$. The iteration count should be kept small to prevent excessive alteration of the latent z_0 as this could potentially affect the visual appearance of the original image. This process is also known as Image2Image editing [11]. In practical terms, we observed that a brief cycle of fixed-point iteration, involving two noise-addition steps (backward process) followed by two denoising steps with the prompt p (forward process), proves effective.

This process is illustrated in Figure 4(b). Here, we pre-process z_0^E by two fixed-point iterations to obtain an improved latent \tilde{z}_0 (red lines). \tilde{z}_0 is decoded to a very similar image x and results with consistent inversion (dashed green lines). For 10k images, we found that the L_2 distance between z_0 and \tilde{z}_0 (i.e., $\|z_0 - \tilde{z}_0\|$) is only 12. This illustrates that the proposed pre-processing method is capable of maintaining a highly consistent backward-forward process.

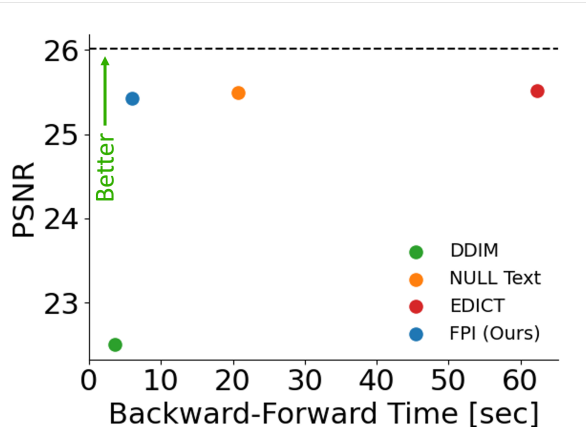


Figure 5. **Inversion Results:** Mean reconstruction quality (y-axis, PSNR) and runtime (x-axis, seconds) of four inversion methods on the COCO2017 validation set. All methods run for 50 denoising steps. Our method reaches high PSNR with $\times 4$ to $\times 12$ shorter inversion-reconstruction time compared to other methods. The dashed line represents an upper bound induced by the VAE. All runtimes are measured on a single A100 GPU.

4. Experiments

We evaluate our approach on three main tasks: (1) **Image inversion and reconstruction:** Here, We assess the inversion fidelity by evaluating the quality of the reconstructed images. (2) **Image Editing:** We show image editing performance using our inversion scheme and, (3) **Rare Concept Generation:** We illustrate how our method can be applied to improve the generation of rare concepts. Code will be made publicly available upon acceptance.

Compared Methods: We compared our approach with the standard **DDIM Inversion** [21] and with two state-of-the-art inversion techniques: (1) **Null-text** [13] which optimizes the null conditioning at every denoising step to accurately invert a given image and, (2) **EDICT** [22], an inversion method based on affine coupling layers. In all experiments, we used code and parameters provided by the authors of the compared methods.

Implementation details: All experiments were conducted with Stable Diffusion v1.5 [16] implemented with Pytorch. Input images were trimmed to make them square and resized to 512×512 . For all approaches, we set the number of sampling steps to be 50 with a stride of 20 over $T = 1000$ diffusion steps. All baselines were run until convergence, while FPI was run for fixed 5 iterations per diffusion step. For a fair comparison, all methods were executed on the same infrastructure (a single A100 GPU), and the experiment runtime was documented accordingly.

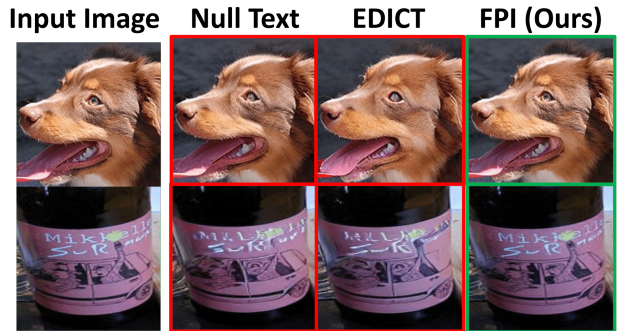


Figure 6. **Image reconstruction, qualitative results :** We show reconstructions of images from MS-COCO, focusing on areas with fine details. At the top row, FPI correctly reconstructs the eye and fur of the dog and at the bottom row, it correctly reconstructs the label text on the bottle (Mikkeller). All baselines were executed until they achieved convergence.

4.1. Image Reconstruction

To evaluate the fidelity of our approach, we measure PSNR of images reconstructed from seed inversions. Specifically, we used the entire set of 5000 images from the MS-COCO-2017 validation dataset [9], along with their corresponding captions. For each image-caption pair, we first found the inverted latent and then used it to reconstruct the image using the same caption. Given that the COCO dataset provides multiple captions for each image, we used the first listed caption as a conditioning prompt.

Figure 5 shows PSNR of reconstructed images in relation to inversion time, demonstrating the performance of our approach compared to state-of-the-art (SoTA) inversion methods. Time is measured on a single NVIDIA A100 GPU for all methods. The dashed black line is the upper bound induced by the Stable Diffusion VAE. It shows that our method is able to achieve comparable PSNR to recent methods and close to the upper bound of VAE, yet accomplishes this in the shortest amount of time. Furthermore, in contrast to other methods, our approach accurately inverts an image to a single latent vector without requiring additional memory. Figures 1 and 6 further demonstrate a qualitative comparison of reconstructed images. We provide in the supplementary material an additional analysis.

Memory Usage: Compared to Null-text [13] and EDICT [22], FPI does not require any additional learnable parameters. In contrast, EDICT requires 16K additional parameters, and Null text necessitates almost 3 million additional parameters for a single image.

4.2. Image Editing

Image editing from text is the task of making desirable changes in certain image regions, well blended into the image, while preserving the rest of the image intact. Current



Figure 7. **Qualitative results of image editing.** FPI edits images more naturally while preserving the structure of the original image. All baselines were executed until they reached convergence, whereas our approach was run for five iterations per diffusion step.

state-of-the-art methods for editing images start by inverting a real image into latent space and then operating on the latent. As a result, the quality of editing depends strongly on the quality of inversion [13].

We now evaluate the effect of inverting images with FPI, compared to state-of-the-art inversion baselines, for complex real image editing. We used Prompt2Prompt [6] as our editing method. All baselines were executed until they reached convergence, whereas our approach was iterated for a fixed number of five iterations per diffusion step (editing in 5 seconds).

We present below both qualitative and quantitative results.

Qualitative results. Figure 1 and 7 give a qualitative comparison between Null-text, EDICT, and FPI in the context of real image editing. FPI excels in accurately editing real

	Null Text	EDICT	FPI (ours)
Percent preferred	18.3%	20.0%	61.7%

Table 1. **User Study:** Values are the percentage of raters that selected each option. N=60 images, of which 12 were provided by the authors of [13] and the rest were randomly sampled from COCO. Raters were asked to select the best editing result in terms of fidelity to both the input image and to an edit instruction.

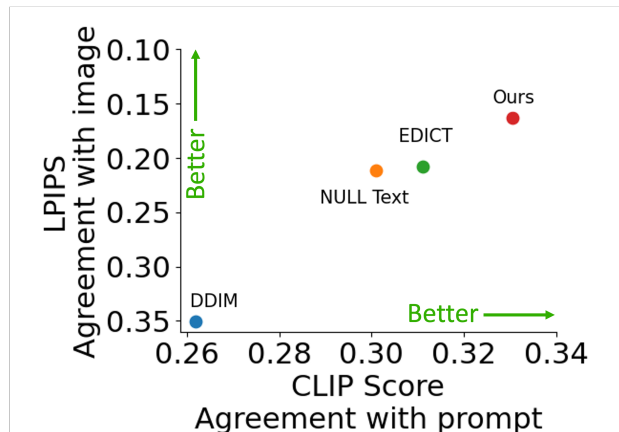


Figure 8. **Semantic quality vs reconstruction quality:** Four inversion methods are compared. Semantic quality is measured using CLIP distance between image and text prompt. The image reconstruction quality is measured using LPIPS distortion score following previous protocols.

images with target prompts producing images with both high fidelity to the input image and adherence to the target prompt. The examples illustrate how alternative approaches may struggle to retain the original structure or tend to overlook crucial components specified in the target prompt. For instance, in Figure 1(right), competing methods largely fail to add the boat as requested. In row 2 of Figure 7, FPI transforms only the bananas into oranges, preserving the appearance of the woman, that hat, and people in the background. In the third row, Null-text [13] eliminates the woman behind the man, and EDICT [22] removes the pile of apples on the left. FPI stands out in altering only the fruits without affecting the rest of the image. More examples can be found in the supplementary material.

User Study. We further evaluated editing quality using human raters. We followed the evaluation process of [13] and asked human raters to rank edits made by three methods. 60 images were rated, 12 images were provided by the authors of [13] and the rest were randomly selected from the COCO dataset [9]. Three raters for each image were recruited through Amazon Mechanical Turk and were tasked to choose the image that better applies the requested text edit while preserving most of the original image. As shown

ImageNet1k in LAION2B

Methods	Many	Med	Few	Total Acc	FID	\hat{T}_{Init}	\hat{T}_{Opt}
	n=235 #>1M	n=509 1M>#>10K	n=256 10K>#			(sec)	(sec)
NAO w DDIM	98.5	96.9	85.1	94.3	6.4	25	29
NAO w FPI (ours)	98.6	97.2	87.3	95.0	6.4	19	26

Table 2. **Impact of inversion quality on the generation of rare concepts:** Image generation quality measured by the accuracy of a pre-trained classifier. We compare NAO [18], a state-of-the-art algorithm when using DDIM inversion (top row), and our FP-inversion (bottom row). Average per-class accuracy is reported separately for the Head (over 1M samples in train set), Medium, and Tail (rare classes below 10K train samples). Our FPI boosts the accuracy of rare and medium concept generation without jeopardizing performance elsewhere.

	Interpolation [19]		Centroid [18]	
	ACC \uparrow	FID \downarrow	ACC \uparrow	FID \downarrow
DDIM Inversion	51.59	6.78	67.24	5.48
FPI (ours)	54.98	5.91	70.18	4.59

Table 3. **Impact of inversion on image interpolation and centroid finding.** (NOA-Path and NOA-centroid [18]). In the interpolation task, two images x^1, x^2 are inverted, and then images are generated along the path between their latent seeds z_T^1, z_T^2 . In centroid-finding, a set of images is inverted and their centroid is found. We measure the quality of generated images by NAO [18] where the only difference is the inversion methods. Acc and FID scores improved considerably when replacing DDIM with FPI.

in Table 1, FPI was favored by raters by a large margin.

LPIPS vs CLIP Score. Following [8, 22], we evaluate the results using two complementary metrics: LPIPS [24] to quantify the extent of structure preservation (lower is better) and a CLIP-based score to quantify how well the generated images comply with the text prompt (higher is better). Metrics are averaged across 100 MS-COCO images, (see Suppl. for details). Figure 8 illustrates that editing with FPI yields a superior CLIP and LPIPS score, demonstrating the ability to perform state-of-the-art real image editing with superior fidelity. It further affirms the findings derived from the user study.

4.3. Seed Interpolation & Rare concept generation

Interpolation and centroid finding: We start by evaluating the benefit of our seed inversions for image interpolation and centroid finding. We follow the experimental protocol of [18] and compare images generated by DDIM with those produced by FPI. Evaluation is conducted based on FID score and image accuracy, assessed using a pre-trained classifier. See details in [18]. Results are presented in Table 3. Notably, in comparison to DDIM inversion, initializing with our seeds consistently results in higher-quality images both in interpolation paths and seed centroids. Vi-

sual illustration can be found in suppl. material.

Rare concept generation: We further show the effect of our seed inversions on the performance of NAO centroids with SeedSelect for rare concept generation. Specifically, we compared images generated by SeedSelect initialized with NAO using DDIM inversion (NAO(DDIM) in Table 2) and using FPI (NAO(FPI)). We followed the evaluation protocol of [18, 19] on ImageNet1k classes arranged by their prevalence in the LAION2B dataset [20]. This dataset serves as a substantial “in the wild” dataset employed in training foundation diffusion models, such as Stable Diffusion [16]. Image quality is measured by FID and accuracy of a pre-trained classifier. For more details see [18, 19].

The results, summarized in Table 2, demonstrate that our inversion method significantly boosts performance, both in accuracy and FID, compared to DDIM inversions. Furthermore, our inversions yield a more precise and effective initialization point for SeedSelect [19], resulting in notably quicker convergence (see Table 2) without compromising accuracy or image quality.

5. Summary

Image inversion in diffusion models is a crucial building block for various applications, including image editing, semantic augmentation, and generating images of rare concepts. The quality of the inverted seed in the noise space significantly affects downstream task performance. Current methods trade off inversion quality with computational cost (runtime, and memory footprint), taking an order of magnitude more compute for high-quality inversion. This paper introduces Fixed-Point Inversion (FPI), a novel method for diffusion inversion of real images that establishes a new point in this trade-off map. FPI revolves around the implicit equation governing the diffusion process, replacing the approximation step with an iterative process involving fixed-point iterations. This approach converges rapidly and demonstrates superior performance in terms of accuracy, execution time, and memory footprint.

We evaluate FPI extensively in three downstream tasks including a) Image inversion and reconstruction, b) Real image editing, and c) Rare concept generation. In all cases, we find that our solution produces improved results compared to the state of the art. This was further supported by a user study, indicating a preference for images edited by our method. Our solution is easy to implement and does not involve additional training, eliminating the need for computationally expensive tuning of the diffusion model.

References

- [1] Yogesh Balaji, Seungjun Nah, Xun Huang, Arash Vahdat, Jiaming Song, Karsten Kreis, Miika Aittala, Timo Aila, Samuli Laine, Bryan Catanzaro, et al. ediffi: Text-to-image diffusion models with an ensemble of expert denoisers. *arXiv preprint arXiv:2211.01324*, 2022. 1, 2, 3
- [2] J. Douglas Burden, Richard L.; Faires. Fixed-point iteration. 1985. 2, 4
- [3] Prafulla Dhariwal and Alex Nichol. Diffusion models beat gans on image synthesis. *NeurIPS*, 2021. 4
- [4] Rinon Gal, Yuval Alaluf, Yuval Atzmon, Or Patashnik, Amit H Bermano, Gal Chechik, and Daniel Cohen-Or. An image is worth one word: Personalizing text-to-image generation using textual inversion. *ICLR*, 2023. 2
- [5] Rinon Gal, Moab Arar, Yuval Atzmon, Amit H Bermano, Gal Chechik, and Daniel Cohen-Or. Designing an encoder for fast personalization of text-to-image models. *arXiv preprint arXiv:2302.12228*, 2023. 2
- [6] Amir Hertz, Ron Mokady, Jay Tenenbaum, Kfir Aberman, Yael Pritch, and Daniel Cohen-Or. Prompt-to-prompt image editing with cross attention control. *arXiv preprint arXiv:2208.01626*, 2022. 2, 7
- [7] Jonathan Ho and Tim Salimans. Classifier-free diffusion guidance. In *NeurIPS 2021 Workshop on Deep Generative Models and Downstream Applications*, 2021. 2
- [8] Inbar Huberman-Spiegelglas, Vladimir Kulikov, and Tomer Michaeli. An edit friendly ddpn noise space: Inversion and manipulations. *arXiv:2304.06140*, 2023. 3, 8
- [9] Tsung-Yi Lin, Michael Maire, Serge Belongie, James Hays, Pietro Perona, Deva Ramanan, Piotr Dollár, and C. Lawrence Zitnick. Microsoft coco: Common objects in context. In *ECCV*, 2014. 6, 7
- [10] Cheng Lu, Yuhao Zhou, Fan Bao, Jianfei Chen, Chongxuan Li, and Jun Zhu. DPM-Solver: a fast ode solver for diffusion probabilistic model sampling in around 10 steps. *Advances in Neural Information Processing Systems*, 35:5775–5787, 2022. 3
- [11] Chenlin Meng, Yutong He, Yang Song, Jiaming Song, Jiajun Wu, Jun-Yan Zhu, and Stefano Ermon. SDEdit: Guided image synthesis and editing with stochastic differential equations. In *ICLR*, 2022. 5
- [12] Daiki Miyake, Akihiro Iohara, Yu Saito, and Toshiyuki Tanaka. Negative-prompt inversion: Fast image inversion for editing with text-guided diffusion models. *arXiv preprint arXiv:2305.16807*, 2023. 2
- [13] Ron Mokady, Amir Hertz, Kfir Aberman, Yael Pritch, and Daniel Cohen-Or. Null-text inversion for editing real images using guided diffusion models. *CVPR*, 2023. 1, 2, 3, 4, 6, 7, 10, 11
- [14] Jorge Nocedal and Stephen J Wright. *Numerical optimization*. Springer, 1999. 4, 13
- [15] Aditya Ramesh, Prafulla Dhariwal, Alex Nichol, Casey Chu, and Mark Chen. Hierarchical text-conditional image generation with clip latents. *arXiv preprint arXiv:2204.06125*, 2022. 1, 2, 3
- [16] Robin Rombach, Andreas Blattmann, Dominik Lorenz, Patrick Esser, and Björn Ommer. High-resolution image synthesis with latent diffusion models. In *CVPR*, 2022. 2, 6, 8
- [17] Chitwan Saharia, William Chan, Saurabh Saxena, Lala Li, Jay Whang, Emily Denton, Seyed Kamyar Seyed Ghasemipour, Burcu Karagol Ayan, S Sara Mahdavi, Rapha Gontijo Lopes, et al. Photorealistic text-to-image diffusion models with deep language understanding. *NeurIPS*, 2022. 1, 2, 3
- [18] Dvir Samuel, Rami Ben-Ari, Nir Darshan, Haggai Maron, and Gal Chechik. Norm-guided latent space exploration for text-to-image generation. *NeurIPS*, 2023. 2, 3, 8, 12, 13
- [19] Dvir Samuel, Rami Ben-Ari, Simon Raviv, Nir Darshan, and Gal Chechik. Generating images of rare concepts using pre-trained diffusion models. *AAAI*, abs/2304.14530, 2024. 2, 3, 8, 13
- [20] Christoph Schuhmann, Romain Beaumont, Richard Vencu, Cade Gordon, Ross Wightman, Mehdi Cherti, Theo Coombes, Aarush Katta, Clayton Mullis, Mitchell Wortsman, et al. LAION-5B: An open large-scale dataset for training next generation image-text models. *NeurIPS*, 2022. 8
- [21] Jiaming Song, Chenlin Meng, and Stefano Ermon. Denoising diffusion implicit models. *ICLR*, 2021. 2, 3, 4, 6
- [22] Bram Wallace, Akash Gokul, and Nikhil Vijay Naik. Edict: Exact diffusion inversion via coupled transformations. *CVPR*, 2022. 1, 2, 3, 4, 6, 7, 8, 10, 11
- [23] Guoqiang Zhang, Jonathan P Lewis, and W Bastiaan Kleijn. Exact diffusion inversion via bi-directional integration approximation. *arXiv:2307.10829*, 2023. 2
- [24] Richard Zhang, Phillip Isola, Alexei A Efros, Eli Shechtman, and Oliver Wang. The unreasonable effectiveness of deep features as a perceptual metric. In *CVPR*, 2018. 8

Fixed-point Inversion for Text-to-image diffusion models

Supplementary Material

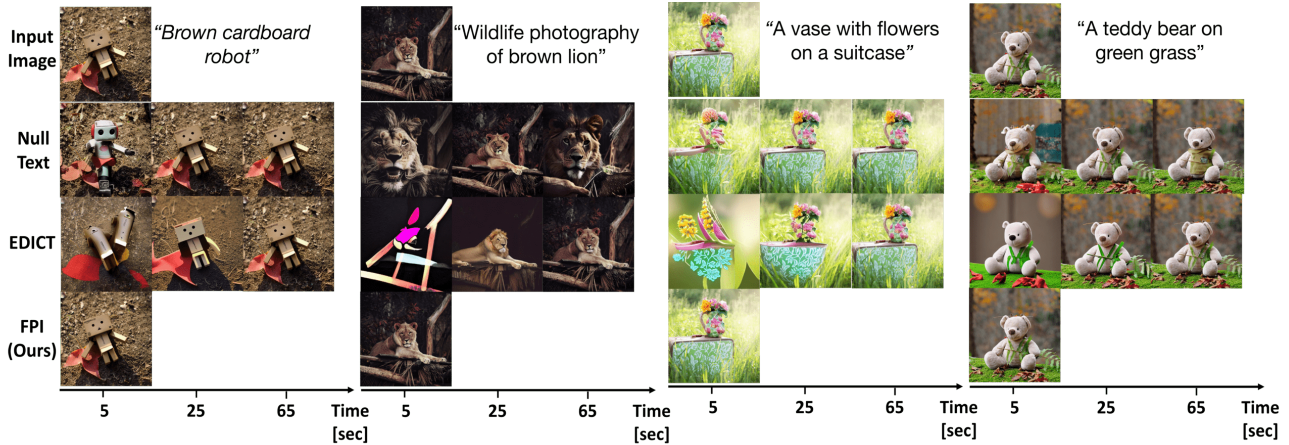


Figure 9. Qualitative and Speed comparison for **image inversion**: The results showcase the speed of FPI compared to SoTA. While FPI completes reconstruction after 5 sec, other alternatives are deeply at their intermediate stages.



Figure 10. Qualitative and Speed comparison for **image editing**: FPI achieves faster and often more plausible editing results while retaining high fidelity to the original image. Column 1: The change to a "Cat" is more realistic. Column 2: The giraffe is well structured. Column 3: While other methods struggle in this case, FPI conducts the editing with a subtle change by creating table "legs" to the suitcase (note the gap between the legs) and making the suitcase top flat, thus changing it to a table without a noticeable change to the rest of the image (e.g. the flowers). Column 4: A case where all methods succeed. Please zoom in for better observation.

6. Additional Qualitative Results

In this section, we present additional qualitative comparisons involving FPI, Null-Text [13], and EDICT [22]. Figure 9 provides insights into inversion-reconstruction, showcasing that FPI converges significantly faster than previous techniques when it comes to image inversion.

Figure 10 compares real image editing. While other methods struggle to achieve proper editing or take a considerable amount of time, our approach delivers desirable

outcomes within 5 seconds. This is illustrated in the first example, where FPI successfully transforms a cardboard robot into a cardboard cat. In contrast, Null-Text does not alter the shape of the robot, and EDICT changes it to a cat, but the result does not appear plausible. In the third example, where the task is to change a suitcase to a table, other approaches fail, while ours subtly changes the suitcase into a table by creating a gap between the sides.

Figures 11 and 12 provide further comparisons for real-image editing. In this context, Null-Text and EDICT were



Figure 11. Qualitative comparison for **image editing A**: One can notice the "under" and "over" editing effects in many cases. Row 1: Null-text changes the food only at the top plate, EDICT looks to miss the change while FPI succeeds. Row 2: Null-text adds a new object to the scene, EDICT, removes the person at the back, and adds a red tint to the woman's hair color. Rows 3 & 4: FPI creates more reliable edits. Row 5: We show a case where all methods struggle to make a plausible editing. Please zoom in for better observation.

executed until convergence, while FPI underwent five iterations per diffusion step. These figures illustrate how alternative approaches may struggle to preserve the original structure or overlook crucial components specified in the target prompt. For example, in the first row of Figure 11, our approach transforms food into flowers, while other methods fail to do so. In the second row, our approach maintains the original placement of the hydrant, whereas Null-Text fails to do so, and EDICT alters the woman's hair to red. Our approach only changes the hydrant to red without modifying the rest of the image. Figure 12 highlights an example of FPI success (clean water instead of dirty) in the third row, where other alternatives totally fail. The last row of Figure 11 depicts a failure of our method, where it could not

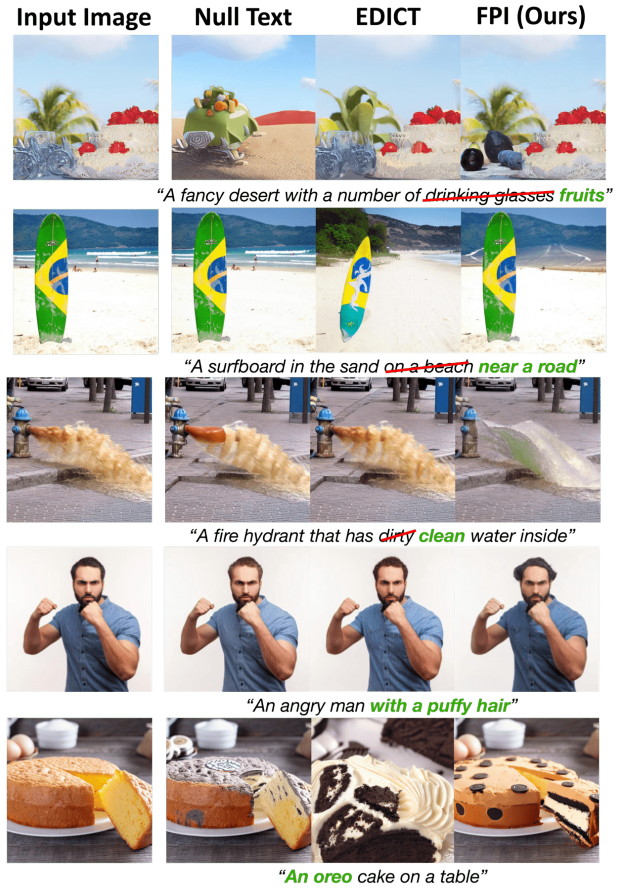


Figure 12. Qualitative comparison for **image editing B**: Note the 3rd row (clean water), where only our FPI was capable of making the correct change.

transform the cake into a hat as requested.

Figure 13 shows the outcomes of various edits on the same image, providing additional confirmation that FPI selectively modifies only the pertinent parts in the image while maintaining the original structure.

7. Restricting Execution Time for Baselines

In this section, we outline additional implementation details regarding the execution time of Null-Text [13] and EDICT [22].

For Null-Text, we constrained the null optimization iterations during each diffusion to achieve the desired convergence limit. Specifically, for a 5-second duration, we set the iterations to 2, and for 25 seconds, we increased it to 10 optimization steps, following the recommendations of the authors.

Concerning EDICT, the number of diffusion steps during generation was restricted to meet the desired time limit as specified in the paper. For a 5-second duration, we ran

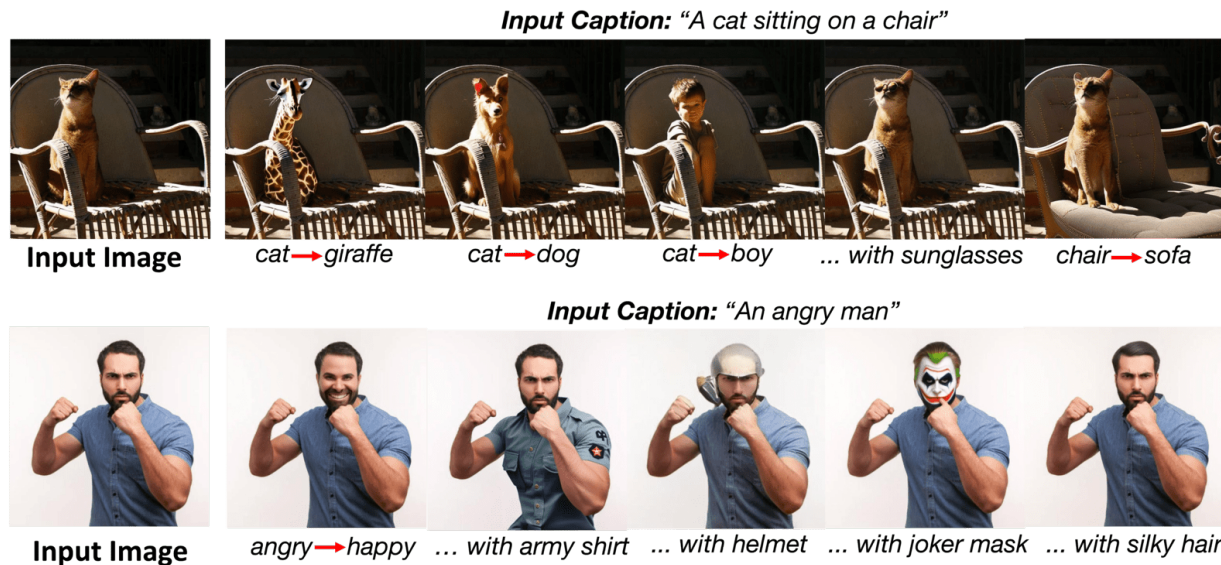


Figure 13. Various editing with same input: Note the FPI capability in both subtle and extensive changes as one would expect from the particular prompt change.



Figure 14. Effect of prompt-aware adjustment on image inversion. Here we show the strong impact of our prompt-aware adjustment on the reconstruction results. Without the adjustment, the results are often unrealistic or far from the original image.

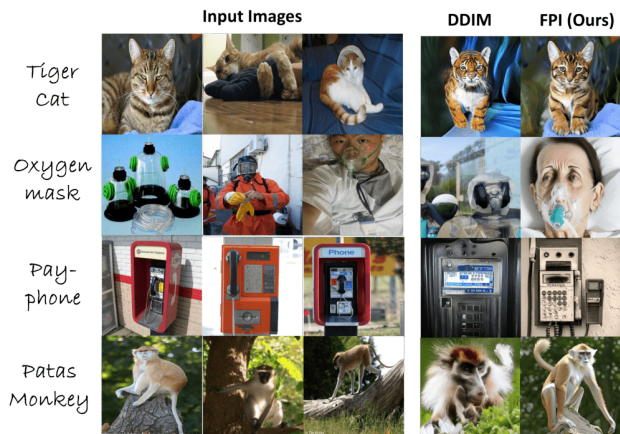


Figure 15. Generating rare concepts based on a few examples with the method of [18] that heavily depends on the diffusion-inversion quality. In our comparison, we evaluate FPI alongside DDIM (refer to the discussion in the main paper). DDIM frequently struggles to produce a realistic representation of certain objects (such as Oxygen-mask or Patas Monkey) or an accurate depiction of specific concepts (like Tiger-cat or Pay-phone). However, the use of FPI rectifies these issues in the results. For a detailed quantitative comparison, please refer to the main paper. See the main paper for a quantitative comparison.

EDICT for 10 steps, and for a 25-second duration, we extended it to 35 diffusion steps, out of the full 50 for complete convergence.

8. Modern Approaches for Solving Implicit Functions

In our paper, we utilized fixed-point iterations to solve the implicit function. While more advanced methods like Newton-Raphson and Conjugate Gradient [14] are available for this purpose, we found them impractical for the following reasons: Newton-Raphson exhibited longer convergence times due to gradient computation, and Conjugate Gradients required finding gradients for latents with a dimension of $4 \times 64 \times 64 \approx 16K$, making it impractical.

9. The Effect of Prompt-Aware Adjustment

Figure 14 presents qualitative results demonstrating the impact of prompt-aware adjustment on image inversion and reconstruction, as proposed in Section 3.3 of the main paper. These results provide qualitative justification for the findings presented in the paper, highlighting that, without prompt-aware adjustment, reconstructed images differ from the original.

10. Rare Concept Generation

Figure 15 displays results for the rare-concept generation task introduced in [18, 19]. The objective is to enable the diffusion model to generate concepts rarely seen in its training set by using a few images of that concept. Both methods in [18, 19] utilize diffusion inversion for this purpose. In the main paper, we presented experiments showcasing the impact of our new inversion process on the outcomes of [18, 19].

Here, we provide qualitative results based on NAO [18] centroid computation when utilizing FPI, contrasting them with those obtained through DDIM inversions. The illustrations demonstrate that FPI is capable of identifying high-quality centroids with correct semantic content compared to centroids found by DDIM.